JOURNAL OF PROPULSION AND POWER
Vol. 18, No. 4, July–August 2002

On-Orbit Optical Observations of Electric Propulsion Space Experiment 26-Kilowatt Arcjet

L. K. Johnson*
The Aerospace Corporation, El Segundo, California 90245
G. G. Spanjers† and D. R. Bromaghim‡
U.S. Air Force Research Laboratory, Edwards Air Force Base, California 93524
M. W. Dulligan§
ERC, Inc., Edwards Air Force Base, California 93524
and
W. A. Hoskins¶
General Dynamics Corporation, Redmond, Washington 98073

During the course of eight flight firings of the ESEX 26-kW arcjet in March and April 1999, optical observations from onboard and ground-based sensors were obtained. Images of the thruster plume at 656 nm confirm expectations that the plume luminescence in the space environment is more compact than that from a thruster operated in the laboratory at higher background pressure. Observations using a ground-based telescope reveal blackbody and line emission spectrum over the range 325–675 nm. The spectral features are consistent with ground tests. Line ratios observed in flight show a moderately higher degree of excitation than ground tests, which is consistent both with the higher specific power and the less collisional plume expansion of the flight test compared to ground tests.

Introduction

A MAJOR goal of the U.S. Air Force Electric Propulsion Space Experiment (ESEX)[1] was to explore integration and performance issues by making measurements on a high-power arcjet in flight. ESEX was launched on 23 February 1999 as one of nine experiments aboard the U.S. Air Force's Advanced Research and Global Observation Satellite (ARGOS), in a sun-synchronous, low Earth orbit of approximately 840-km altitude and 99-deg inclination.[2] Two optical emission diagnostics were successfully applied during flight firings in March and April 1999. An onboard charge-coupled device (CCD) camera was employed to provide visual confirmation of proper operation of the arcjet and qualitatively observe plume and nozzle heating phenomena during firings. A ground-based spectrograph and telescope were used to gather emission spectra, proving the concept of ground-based spectroscopy of spacecraft and allowing for comparison of flight data to ground-test data. Other diagnostic sensors sensitive to optical signals aboard the spacecraft include two instrumented solar cells and four radiometers. Because these sensors were intended as contamination monitors, descriptions and results are given for them in the associated ESEX contamination papers by Spanjers et al.[3] and Schilling et al.[4]

Received 22 January 2001; revision received 7 February 2002; accepted for publication 27 January 2002.

*Electric Propulsion Space Experiment Chief Scientist; currently Research Scientist, Thermal and Propulsion Engineering Department, Jet Propulsion Laboratory, Mail Stop 125-109, 4800 Oak Grove Drive, California Institute of Technology, Pasadena, CA 91109; lee.k.johnson@jpl.nasa.gov. Member AIAA.

†Project Scientist, Propulsion Directorate, 1 Ara Road. Member AIAA.

‡Electric Propulsion Space Experiment Program Manager, Propulsion Directorate, 1 Ara Road. Member AIAA.

§Project Scientist, 1 Ara Road. Member AIAA.

¶Project Engineer, Ordnance and Tactical Systems, P.O. Box 97009. Member AIAA.

Video Camera

The video still camera consists of an optical train to focus and filter light from the arcjet, a CCD focal plane to capture the image, and associated electronics to control the camera and readout. The optical train consists of a heat-blocking filter and a narrowband interference filter centered at 656 nm, which is the wavelength of the 3p-2s Balmer-alpha ($H\alpha$) transition of excited atomic hydrogen. Laboratory studies of ammonia arcjets show that this wavelength dominates the visible plume.[5] Although excited atomic hydrogen is a minor plume constituent, no other emission line in the CCD range of sensitivity yields more information, and the Balmer-alpha line has been well studied in laboratory tests. The camera field of view is shown in Fig. 1. The focal plane consists of a 758×486 conventional CCD. An electronic shutter controls the CCD exposure to arcjet light; ground commanding is available to program each frame's exposure over the range from 1/60 to 1/10,000 s. The camera electronics unit reads and temporarily stores frames from the CCD. A maximum of 22 frames of video data may be stored in the camera electronics before readout, which functionally serves as a limit to the number of exposures possible during an arcjet firing.

Spectrograph/Telescope

The ground-based optical instruments integrated specifically for ESEX consist of a spectrograph and CCD detector fed by one of the Air Force's telescopes on Maui. The telescope belongs to a joint Air Force Research Laboratory/Air Force Space Command unit and was made available on a visiting experimenter basis. The telescope is located on Haleakala Crater, Maui [Maui Space Surveillance Site (MSSS)] at an altitude of 3048 ft. The pertinent optical elements consist of a 1.6-m-diam aluminized parabolic primary mirror and a hyperbolic secondary mirror feeding a conventional Cassegrain focus of $f/16$ approximately 76 cm beyond a rear mounting surface. The mount has three axes of control, consisting of a conventional polar/declination astronomical arrangement mounted on top of an azimuth table. The facility is described in publications of the U.S. Air Force Research Laboratory.[6]

The ESEX instrument package, mounted to the rear surface, consists of auxiliary optics, the spectrograph, a slit tracking camera, the CCD at the focal plane of the spectrograph, and associated

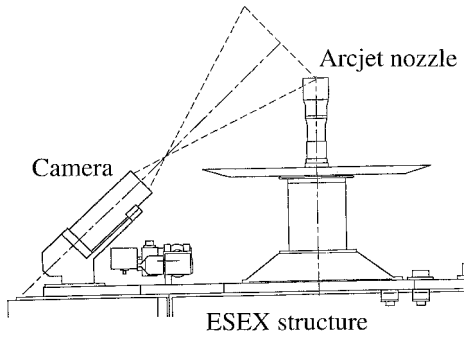

Fig. 1 ESEX thruster and video still camera field of view.

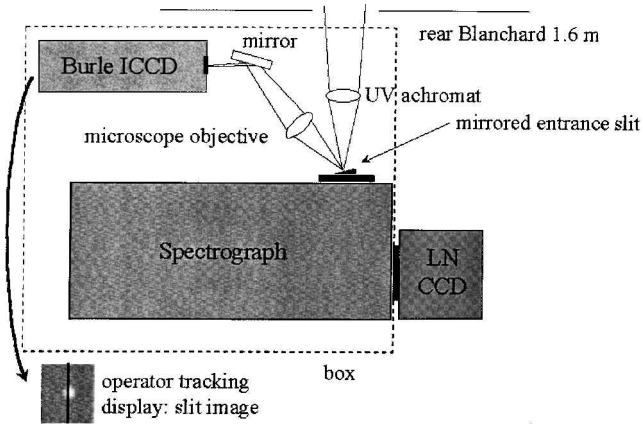

Fig. 2 Schematic diagram of spectrograph, detector, and slit camera.

electronics. An optical schematic is presented in Fig. 2. On the way to the entrance of the spectrograph, light from the telescope passes through a filter wheel. This filter wheel holds a ground glass square, which is rotated into the spectrograph field of view and illuminated by mercury and neon emission lamps for wavelength calibration. After the filter wheel, the $f/16$ converging beam passes through a doublet achromatic lens of 200-mm focal length to f-number match the beam to the $f/7$ spectrograph. Focusing of the telescope secondary is used to bring the image into focus on the entrance slit of the spectrograph.

The spectrograph entrance is a custom assembly consisting of a slit piercing a flat, mirrored surface, which is angled 20 deg about an axis parallel to the slit length. Consequently, light not entering the spectrograph is reflected at 40 deg from the entrance axis to a reimaging lens consisting of a 50-mm focal length microscope objective. The converging beam leaving the microscope objective transits a fold mirror and falls on an intensified video-rate CCD. This slit tracking camera is used with the telescope pointing controls to direct the very small image of the spacecraft into the slit. A typical image of a calibration star or spacecraft on the spectrograph entrance slit is approximately 50 μm in extent, corresponding to less than 1 arc-s. The extra control afforded compensates for errors in the spacecraft orbital elements used to point the telescope and for image drift from atmospheric refraction.

An aperture is used at the spectrograph entrance for intensity calibration, which does not require high wavelength resolution. Rather, the intent is to capture an entire star image for the total duration of the calibration exposure. A 600-μm aperture (approximately 10 arc-s) was used; an aperture is preferred over a slit to reduce background light. On the other hand, observations of the arcjet plume do require good wavelength resolution, and so a slit 50 μm wide by about 10 mm high was employed, which proved to be a good balance between throughput and resolution. The narrow slit required the telescope operators' best efforts to direct the wavering image continually into the slit by making small adjustments to the telescope tracking.

The slit width also determines the spatial resolution at the target. At a minimum range of 840 km, the 50-μm entrance slit corresponds to approximately 3 m. Because the light emitting part of the ESEX plume is observed in ground test[7] to be approximately 1 m in size, emission from the full extent of the plume, as well as the nozzle radiation, is collected in a measured spectrum.

The spectrograph itself consists of an Acton SP-500 nonimaging spectrometer. The spectrograph was modified to optimize the integration, but the factory configuration of the principal optical elements is satisfactory for operation in any orientation, even inverted. The modifications consist of addition of an internal electronically controlled mechanical shutter just inside the entrance slit, addition of mounting holes in the base, and a tie-down for the swinging exit fold mirror. The spectrograph was also purged continually with dry gaseous nitrogen to prevent condensation.

The detector consists of a Princeton Instruments back-illuminated, VISAR-coated, liquid nitrogen-cooled slow scan CCD with all-orientation dewar. The CCD format is 330 pixels along the slit axis by 1100 pixels along the wavelength axis; the pixel size is 25 μm. This CCD affords good sensitivity, on-chip binning, and very low noise. Performance trades indicated that this LN liquid nitrogen CCD would provide better signal to noise ratio than an intensified CCD for ESEX observations. The detector controller is mounted on the telescope adjacent to the spectrograph and passes CCD data over a serial interface to the remotely located data acquisition computer located approximately 30 m from the telescope. Several other displays are provided to the observer at the computer location, including video displays of mount parameters, finder telescope image, and slit tracking camera image.

Observing runs consist of equipment checks, mount position calibration, wavelength calibration, focus adjustment, and data acquisition runs for either star intensity calibrations or arcjet firings. For star tracks, the catalog position of the calibration star is input to the mount computer, the mount is set to follow the sidereal motion, and the star is identified on the 30 arc-min finder telescope display. The star image does not usually appear immediately on the slit tracking camera, and so the mount position is then biased while continuing to track sidereally, to direct the image onto the tracking camera and then into the slit. For satellite tracks, the mount computer reads a two-line spacecraft element set (a snapshot of position and velocity at a single time), predicts a corresponding ballistic trajectory, and points the mount accordingly. Both tracking modes continuously improve their automated tracking using real-time operator bias input. For satellite tracks, the azimuth table of the telescope is generally rotated so that the telescope's polar axis is more or less perpendicular to the satellite's path. This allows the tracking motion to be principally in the polar axis, which mimics the astronomical tracking for which the mount structure and stability is optimized.

For arcjet firing observations, a dry run of the mount tracking motion was performed before the event, and for some runs, background sky data were acquired during this dry run pass. For other tracks, the mount positions corresponding to the acquisition times of good data files were recorded, and then the mount was directed to the same positions soon after the satellite track was complete for backgrounds. A communications net was maintained among the ESEX operators at Kirtland Air Force Base and the telescope/spectrograph operators at MSSS. This net allowed operators to be certain the arcjet was on when tracks were being attempted and facilitated inter- and intrasite operations.

Observations

The onboard camera revealed plume emission at Hα and heated nozzle glow as expected. A representative series of images acquired as the arcjet heated up is provided in Fig. 3. No radiance calibration data are available for the camera. Qualitatively, the distribution of radiation intensity observed on the nozzle is similar to that from photographs of the thruster operating in ground tests; however, the plume in ground tests is larger and more confined to the thrust axis than in flight. The flight plume appears to be symmetric as well.

During the spring of 1999, for ARGOS descending node passes at night, the sun did not illuminate the spacecraft as it rose at MSSS. Further, operational constraints prevented arcjet starts before rise, for the available passes; thus, the telescope track either had to be

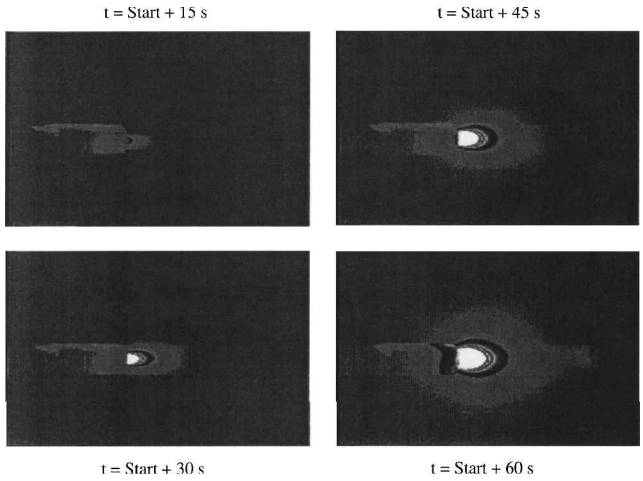

Fig. 3 Series of images acquired from the onboard video camera showing the ramp to full power.

started in the blind or with assistance from an Air Force radar nearby. Both radar tracking and blind tracking worked well in practice, but blind tracking required careful selection of recent spacecraft element sets.

Maui weather that spring also proved to be problematic. Most nights during the available operations interval were unsatisfactory by MSSS standards, due to cloud layers above the observatory, and for many nights, the observatory was shrouded in fog. The small number of clear nights and the arcjet battery charging-cycle schedule[1] together limited the observation opportunities considerably. Star calibrations were performed during the clear nights when the arcjet was not available and during arcjet firing nights, as appropriate, when not preparing for the track.

Preliminary star calibration data for the wavelength range 320–670 nm using a 150 line/mm grating were obtained using the star Feige 110. The calibration so derived does compensate for spectrograph and detector variations and atmospheric losses as a function of wavelength, but not as a function of elevation angle; this preliminary calibration is accurate to ±15%. An approximately 10× loss in sensitivity toward the UV, where the NH (A–X) spectrum is located, is approximately half due to grating blaze and half due to greater atmospheric attenuation in the UV.

Unfortunately, the weather and battery problems[1] combined to preclude four of five planned observations of the arcjet firing. However, the fifth firing was successfully observed at approximately 0250 hrs local time on 26 March, which was a night with thin high clouds. Absorption from these clouds precludes an accurate absolute radiance analysis, but because thin clouds typically absorb equally at different wavelengths,[6] a relative intensity calibration could be done. For this pass, the three-quartermoon was setting at about 1-deg elevation at 288 deg in the northwest. The pass geometry involved a maximum elevation of about 83 deg at 286 deg azimuth, so that the included angle between vectors to the moon and spacecraft from Maui was about 82 deg. This geometry unfortunately allowed the moon to illuminate the high clouds, producing a significant background in the observations.

During the arcjet firing, 14 exposures of the pass were obtained; of these, the first 10 show structure associated with arcjet operation. Early in the pass, the arcjet, located on the ram surface of ARGOS, is visible, but later in the pass, the spacecraft structure progressively obscures the arcjet nozzle and then the plume. The last four exposures occurred when the nozzle and plume were obscured. The spectrograph was set to record a 320–670 nm wavelength range with a 150 line/mm grating blazed at 500 nm. The signal observed during the firing consists of continuum radiation from the hot-nozzle body peaking to the red of 670 nm along with discrete emission lines observed from 325 to 650 nm. Exposures where arcjet signals were unambiguously recorded are shown in Figs. 4 and 5, and a summary of pertinent arcjet parameters for this firing is shown in Fig. 6. The

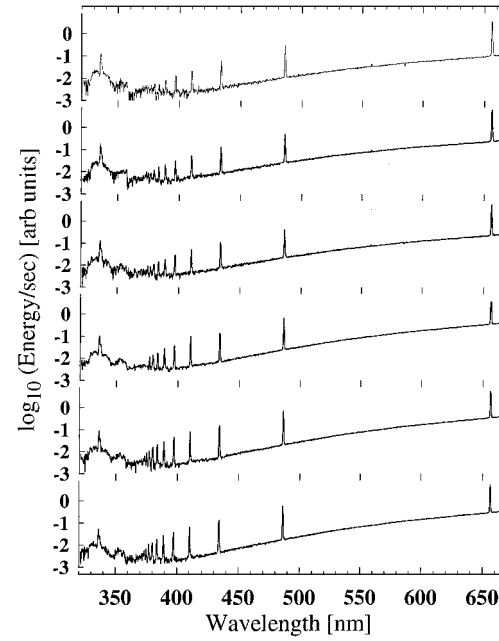

Fig. 4 ESEX arcjet emission spectra, with time during the observation pass increasing from top to bottom.

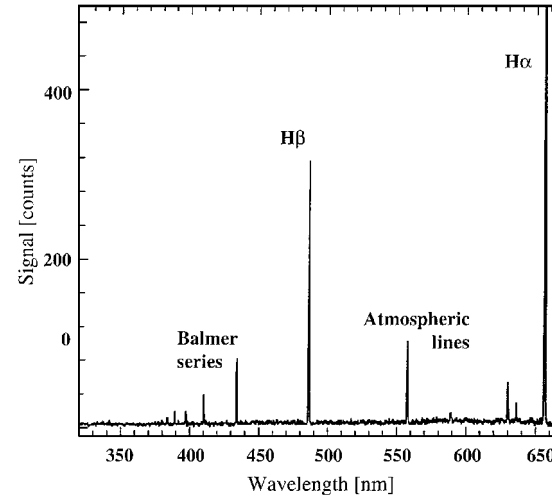

Fig. 5 Isolated plume spectrum.

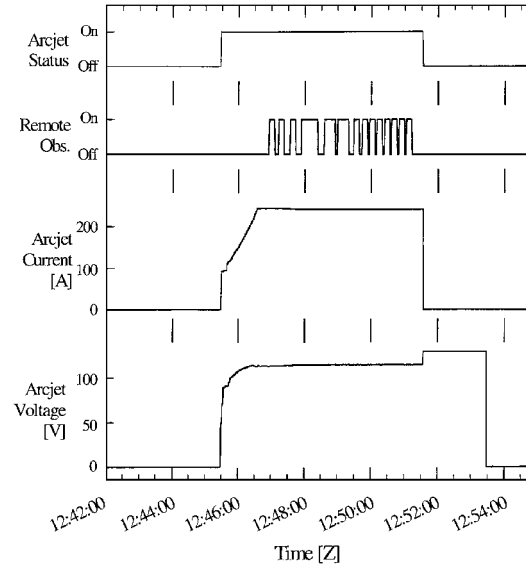

Fig. 6 Arcjet parameters for firing 5; second line shows when observations from spectrograph were obtained.

arcjet was operating stably by the time the first emission data were obtained, and as the pass progressed, the signal stayed about the same until the emission became obscured by the spacecraft body. In Fig. 5, late in the pass, the spacecraft has obscured the nozzle emission, but not yet the plume, so that only the plume emission lines are observed. The vertical scale in Figs. 4–6 is relative energy, from a relative, rather than absolute application of the star intensity calibration.

Analysis

The principal emission lines observed correspond to the atomic hydrogen Balmer series and the NH (A–X) molecular electronic transition and to some smaller, less distinct structures. The results show many of the same features as high-power ammonia arcjet emission spectra taken in ground tests.[7,8]

The Balmer series is visible up to $n = 9$, and no other transitions are seen in the Balmer limit region. The series terms become less intense as the excitation increases, which is consistent with previous observations of high- and low-power arcjets.[9,10] These flight data may be compared with ground-test emission measurements gathered under the ESEX program by Olin/Rocket Research Corporation (RRC) (now General Dynamics Corporation), the arcjet manufacturer.[6] The ground-test data were obtained operating the arcjet into a chamber pressure above 10 mtorr, and the observations imaged a 0.02-in. wide region 0.11 in. downstream of the arcjet exit plane, transverse to the flow. These ground-test data were obtained using a developmental arcjet geometry similar to ESEX.[11] For ground-test measurements above 385 nm, arcjet constrictor (3.8 mm), cathode gap (6.1 mm), and flow rate (240 mg/s) matched ESEX. For ground-test measurements below 385 nm, the arcjet had a slightly different nozzle constrictor (5.1 mm) and cathode gap (6.6 mm) and used 300 mg/s of ammonia. The flow rate change for UV measurements thus represents a 20% reduction in specific power. The relative strengths of the emission features are presented in Table 1 for the ground and flight tests. The two tests show similar results in that the Hα and Hβ lines dominate in both. Differences in NH and H7–H9 emissions can be accounted to differences between flight and ground tests. However, relative differences in ratios between Hα and Hβ–H6 appear to be real, which is interesting.

Previous collisional radiative modeling[7,9] of arcjet Balmer series emission indicated that higher-order terms are in better equilibrium with the (hot) ionized fraction of the plume, whereas the populations of lower terms follow the H atom density and temperature. In these models, radiation trapping and nonequilibrium effects reduce Hα, Hβ, and Hγ emission as H atom and electron density decrease, but do not affect higher terms. This would lead to relatively stronger high-lying terms in the more rarefied plume expansion of the flight experiment, consistent with the observations. It is also likely that emission from the flight plume is less affected by downstream collisional effects and is, thus, more representative of conditions near the hot-plasma arc.

The other large signal observed in the flight data is the NH (A–X) complex whose central peak and wings constitute electronic transitions among vibrational and rotational states. In ground tests, the NH manifold has been compared to equilibrium conditions using Boltzmann temperature analysis (see Refs. 5 and 12–14). These previous analyses concluded that although the NH manifold exhibits a poorly defined equilibrium shape, best-fit Boltzmann rotational and vibrational temperatures can be used to indicate the relative amount of excitation. In particular, previous analysis found an A state vibrational temperature of about 2500 K (Refs. 5 and 14) in reasonable agreement with an X state vibrational temperature of 2200 K determined by laser-induced fluorescence.[13] Previous workers also found an A state rotational temperature of 5000 K (Ref. 12), significantly higher than the X state temperature, also measured using laser-induced fluorescence,[13] of 1650 K. The higher A state rotational temperature is attributed to resonance reabsorption of upstream hot NH emission.[13] The ESEX flight data were analyzed by synthesizing a Boltzmann equilibrium spectrum and fitting the Boltzmann temperature to the observations. In common with ground-test results, the ESEX flight spectra exhibit nonequilibrium features, and in particular show no contribution form $v = 2$ states, whereas the ratio of $v = 0$–1 in the Q branch is best fit by a vibrational temperature of 5000 K. This higher temperature,

Table 1 Arcjet relative emission

Feature	Wavelength, nm	Flight test, %	Ground test, %
NH (A–X)	327–345	5.9	1.9[a]
N_2, N_2^+	348–360	0.5	
H9	377	0.11	1.3[a]
H8	380	0.18	
H7	384	0.25	
H6	389	0.38	0.11
Hε	397	0.57	0.22
Hδ	410	1.5	0.48
Hγ	434	2.2	1.5
Hβ	486	9.5	7.0
Hα	656	78.9	87.5

[a]Non-ESEX arcjet configuration; see text.

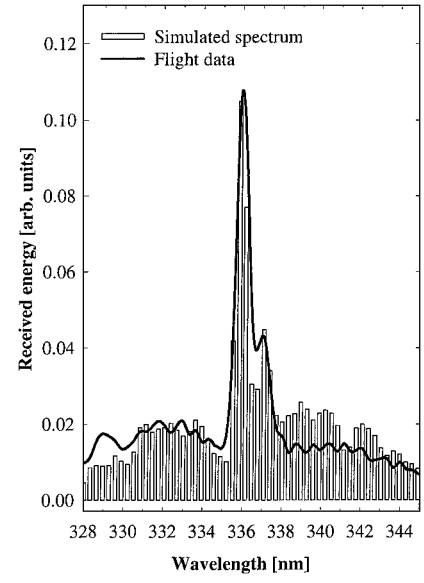

Fig. 7 Flight data and simlated NH spectrum for $T_v = 5000$ K and $T_r = 6000$ K, using $v = 0$, 1, and 2.

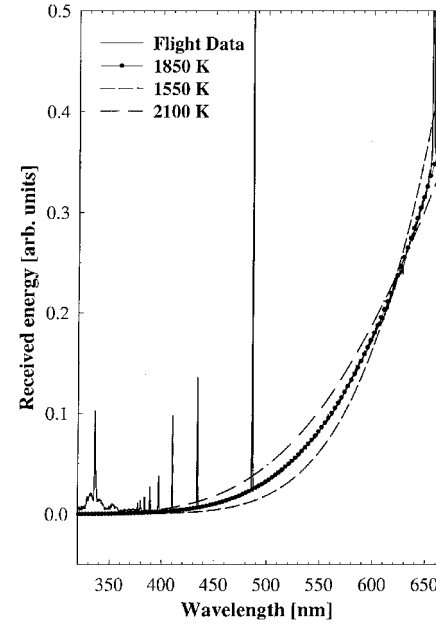

Fig. 8 Blackbody fit to arcjet nozzle emission flight data.

compared to previous studies, is a likely result of the plume expansion in space being less collisional than in the laboratory. Therefore, less vibrational relaxation is expected, and the temperature reflects the hotter conditions near the arc where the NH excited states are produced. For the rotational states, the best fit to the data is for approximately 6000 K, in reasonable agreement with previous work.[13] The flight data and equilibrium prediction, through $v = 2$, is shown in Fig. 7. In Fig. 7, the $v = 2$ Q-branch contribution causes the equilibrium prediction to lie above the flight data for 338–342 nm.

The small features observed in the flight data around 355 nm have not been identified, although some similar, though not identical, lines associated with N_2(C–B) and N_2^+(B–X) are associated with this region and are present in arcjet ground-test data.[7]

An analysis was done to scale the nozzle continuum radiation to a blackbody energy distribution using temperature as a variable parameter. The results of this fit are shown in Fig. 8 for the exposure with the best statistics. The best-fit temperature is 1850 ± 50 K; this can be compared to a measured maximum nozzle temperature in ground test of 2100 K and a predicted thermal model temperature of 1550 K (Ref. 15). Estimated uncertainties in the relative intensity calibration cannot account for the discrepancy between the ground and space measurements; rather, it is likely that the flight measurements show more efficient radiative cooling to the space environment. No attempt can be made to establish the emissivity of the radiating surface because the unquantifiable absorption of the clouds in the flight observations precludes an absolute radiance calibration.

Summary

Optical emission diagnostics, both onboard and remotely based, were applied to the flight of the ESEX arcjet. The onboard imaging camera confirmed operation of the arcjet and showed that the emitting plume in space is smaller than in ground test. The remote spectroscopic measurements proved the concept of ground-based measurements of low-flow advanced thruster plumes. The spectroscopic data generally show a higher degree of excitation compared to ground test, which is likely related to both the high specific power of the flight arcjet and to the reduced number of thermalizing collisions in the flight plume expansion compared to ground-test conditions.

Acknowledgments

The authors acknowledge the inputs from the TRW/RRC team in the design and characterization of the flight sensor package and ground-based thruster measurements. In addition, significant design and integration of the spectrometer package was obtained from the U.S. Air Force Maui optical site team, including the contributions of Jack Albetski in particular.

References

[1]Bromaghim, D. R., LeDuc, J. R., Salasovich, R. M., Spanjers, G. G., Fife, J. M., Dulligan, M. J., Schilling, J. H., White, D. C., and Johnson, L. K., "Review of the Electric Propulsion Space Experiment Program," *Journal of Propulsion and Power*, 2002; also AIAA Paper 99-2706, June 1999.

[2]Turner, B. J., and Agardy, F. J., "The Advanced Research and Global Observation Satellite (ARGOS) Program," AIAA Paper 94-4580, Sept. 1994.

[3]Spanjers, G. G., Schilling, J. H., Bromaghim, D. B., and Johnson, L. K., "Radiometric Analysis from the 26-Kilowatt Electric Propulsion Space Experiment," *Journal of Propulsion and Power*, 2002.

[4]Schilling, J. H., Spanjers, G. G., Bromaghim, D. B., and Johnson, L. K., "Solar Cell Degradation During the 26-Kilowatt Electric Propulsion Space Experiment Flight," *Journal of Propulsion and Power*, 2002.

[5]Manzella, D. H., Curran, F. M., Myers, R. M., and Zube, D. M., "Preliminary Plume Characteristics of an Arcjet Thruster," AIAA Paper 90-2645, July 1990.

[6]"AMOS User's Manual," U.S. Air Force Phillips Lab., 1996 (available from U.S. Air Force Research Laboratory, Kirtland Air Force Base, NM.

[7]Hoskins, W. A., "High Power AJ Spectroscopy Analysis," Final Rept., Olin/Rocket Research Corporation, Redmond, WA, 30 kW Arcjet Analysis, Dec. 1996.

[8]Tosti, E., Mazzacurati, V., Ruscco, G. C., and Deininger, W. E., "Emission Spectroscopy of 15-kWe Arcjet Plumes," AIAA Paper 90-2646, July 1990.

[9]Hoskins, W. A., Kull, A. E., and Butler, G. W., "Measurement of Population and Temperature Profiles in an Arcjet Plume," AIAA Paper 92-3240, July 1992.

[10]Crofton, M. W., "Spectral Irradiance of the 1-kW Arcjet Thruster from 80 to 500 nm," AIAA Paper 92-3237, July 1992.

[11]Cassady, R., and Lichon, D., "Performance Improvement of a 26 kWe Ammonia Arcjet," International Electric Propulsion Conf., IEPC Paper 90-2532, July 1990.

[12]Crofton, M. W., "Advanced Diagnostics of Arcjets," International Electric Propulsion Conf., IEPC Paper 91-095, Oct. 1991.

[13]Crofton, M. W., Welle, R. P., Janson, S. W., and Cohen, R. B., "Rotational and Vibrational Temperatures in the Plume of a 1-kW Ammonia Arcjet," AIAA Paper 91-1491, June 1991.

[14]Janson, S. W., Welle, R. P., Schultess, D. R., and Cohen, R. B., "Arcjet Plume Characterization Part 2: Optical Diagnostics Results," AIAA Paper 90-2643, July 1990.

[15]Kriebel, M. M., "30 kW Class Arcjet Advanced Technology Transition Development (ATTD)," U.S. Air Force Research Lab., Rept. AFRL-PR-ED-TR-1999-0034, Edwards AFB, CA, June 2000.